Available online at www.sciencedirect.com
ScienceDirect
Biochimica et Biophysica Acta 1768 (2007) 155–166
Biochimica et Biophysica Acta BBA
www.elsevier.com/locate/bbamem

Spatial and temporal Ca^{2+}, Mg^{2+}, and ATP^{2-} dynamics in cardiac dyads during calcium release

Ivan Valent [a], Alexandra Zahradníková [b], Jana Pavelková [b], Ivan Zahradník [b,*]

[a] Department of Physical and Theoretical Chemistry, Faculty of Natural Sciences, Comenius University, Bratislava, Slovakia
[b] Institute of Molecular Physiology and Genetics, Slovak Academy of Sciences, Bratislava, Slovakia

Received 1 June 2006; received in revised form 10 August 2006; accepted 17 August 2006
Available online 8 September 2006

Abstract

We have constructed a three-dimensional reaction-diffusion model of the mammalian cardiac calcium release unit. We analyzed effects of diffusion coefficients, single channel current amplitude, density of RyR channels, and reaction kinetics of ATP^{2-} with Ca^{2+} and Mg^{2+} ions on spatiotemporal concentration profiles of Ca^{2+}, Mg^{2+}, and ATP^{2-} in the dyadic cleft during Ca^{2+} release. The model revealed that Ca^{2+} concentration gradients persist near RyRs in the steady state. Even with low number of open RyRs, peak $[Ca^{2+}]$ in the dyadic space reached values similar to estimates of luminal $[Ca^{2+}]$ in ~1 ms, suggesting that during calcium release the Ca^{2+} gradient moves from the cisternal membrane towards the boundary of the dyadic space with the cytosol. The released Ca^{2+} bound to ATP^{2-}, and thus substantially decreased ATP^{2-} concentration in the dyadic space. The released Ca^{2+} could also replace Mg^{2+} in its complex with ATP^{2-} during first milliseconds of release if dissociation of MgATP was fast. The results suggest that concentration changes of Ca^{2+}, Mg^{2+}, and ATP^{2-} might be large and fast enough to reduce dyadic RyR activity. Thus, under physiological conditions, termination of calcium release may be facilitated by the synergic effect of the construction and chemistry of mammalian cardiac dyads.

Keywords: Reaction-diffusion model; Calcium release unit; Calcium signaling

1. Introduction

In myocytes of working mammalian myocardium, a large portion of calcium required for contraction is released from terminal cisterns of sarcoplasmic reticulum (SR). Terminal cisterns form specialized structures with the sarcolemma, known as dyads, which represent mutually independent calcium release units that generate elementary calcium release events [1–4]. The gap between the sarcolemmal and cisternal membrane, ~15 nm wide [5], is filled with the cytoplasm. There, approximately 30–250 ryanodine receptors (RyRs) are clustered on the SR membrane in a regular two-dimensional lattice [6]. In addition to rapid and steeply concentration-dependent regulation by calcium [3,7,8], RyR activation is controlled also by Mg^{2+} ions [9,10–13].

Ca^{2+} ions released through RyRs diffuse through the dyadic space and bind to mobile and immobile calcium buffers [14]. Both Ca^{2+} and Mg^{2+} form weak complexes with adenosine triphosphate (ATP^{2-}) that dissociate rapidly [15]. Additionally, ATP^{2-} is also well known as RyR regulator that substantially increases the probability of RyR opening [16,17]. Therefore, the knowledge of spatial and temporal development of all these three species is necessary to understand activity of release units during activation and termination of calcium release, the exact molecular mechanisms of which are far from being clearly understood (see [3,7,8] for review). Inasmuch as the phenomena occurring at the scale of nanometers within the dyadic cleft are not directly observable by existing techniques, mathematical modeling is used for analyses of hypotheses on calcium release mechanisms [18–20].

Models of calcium diffusion and binding in the cytosol have been used for theoretical reconstruction of calcium sparks to

* Corresponding author. ÚMFG, SAV, Vlárska 5, 833 34 Bratislava, Slovakia. Fax: +4212 5477 3666.
E-mail address: ivan.zahradnik@savba.sk (I. Zahradník).

0005-2736/$ - see front matter © 2006 Elsevier B.V. All rights reserved.
doi:10.1016/j.bbamem.2006.08.020

determine the time course and amplitude of calcium release flux in cardiac calcium release units. Due to incomplete understanding of the kinetic properties of cytoplasmic components, different groups [21–29] arrived at calcium flux estimates ranging widely in amplitude (2–50 pA), duration (5–10 ms), time course (time-invariant or exponentially decaying amplitude), and number of RyRs involved (2–30 channels). Interpretation of the experimental results is thus very strongly dependent on models and their parameters. Nevertheless, these estimates demarcate the most probable range of dyadic calcium release flux amplitudes and durations.

A deeper insight into calcium movement and buffering in the dyadic cleft has been obtained from theoretical treatment of Ca^{2+} fluxes through various pathways (DHPR channel, Na–Ca exchanger, cisternal SR membrane) not accounting for individual gating events. Langer and Peskoff [30] built a radially symmetric one-dimensional model of the dyadic cleft during calcium release. In this study, Ca^{2+} concentration in the center of the dyadic space was estimated to peak at 0.6 mM and to decline to the diastolic level (100 nM) within 150 ms. Soeller and Cannell [31] solved 2D electrodiffusion of Ca^{2+} from a single DHPR channel in a cylindrical model of dyadic cleft. For a DHPR current of 0.2 pA, $[Ca^{2+}]$ at the center of the dyadic space reached peak levels of ~73 μM and descended to the initial value within ~10 ms after the channel closure.

Another approach involved the kinetics of DHPR and RyR gating and of Ca^{2+} buffering. Ordinary differential equations (ODEs) describing a set of cell compartments were used alone [32,33] or in combination with Monte-Carlo simulation of channel gating [34–36] to simulate whole-cell membrane currents or action potentials and cytosolic calcium transients. Alternatively, partial differential equations (PDEs) were used to describe spatial distribution and movement of the involved reactants simultaneously with stochastic generation of individual gating events [18,37]. Due to the large computational expense of this approach, simplified PDE systems with reduced dimensionality were used. It has been shown [37] that RyRs can respond rapidly (~0.4 ms) to calcium influx via DHPRs. Possible allosteric interactions between RyRs were proposed to assure stable excitation–contraction coupling [18].

The aim of this study was to create a three-dimensional (3D) reaction-diffusion model of the cardiac dyad and to examine the spatial and temporal evolution of concentrations of Ca^{2+}, Mg^{2+} and ATP^{2-}, the species involved in calcium signaling, after the onset of calcium release. We analyzed the effect of diffusion, single-channel current amplitude, and number of active RyRs on the spatial and temporal dynamics of Ca^{2+}, Mg^{2+}, and ATP^{2-} in the dyadic space and the surrounding cytosol. The model provided estimates of development and dissipation of calcium concentration after opening and closure of the RyR cluster. We show that free Mg^{2+} and ATP^{2-} concentrations rapidly respond to calcium dynamics and may alter considerably. We propose that the amplitude and dynamics of Ca^{2+}, Mg^{2+}, and ATP^{2-} concentration changes may modulate RyR activity during calcium release.

2. Methods

2.1. Biophysical model of the dyad

The dyadic cleft was modeled as a rectangular domain of 240 × 240 × 15 nm surrounded by cytoplasmic environment (Fig. 1). The ryanodine receptors were represented on the SR membrane as point sources of Ca^{2+} influx forming a lattice with 30 nm spacing [6].

In the basic model, the unitary single RyR channel current was set to 0.36 pA [38,39]. Calcium release was simulated as simultaneous opening of all RyRs in the cluster, lasting 10 ms. There is currently no consensus about the time course and size of calcium release flux and the number of open RyRs during an elementary calcium release event. Therefore, we have modeled calcium release as a constant flux lasting 10 ms [40]. The dyadic space could accommodate 49 densely packed RyRs. Calcium release was modeled first as synchronous opening of 49 RyRs. The amplitude of single-channel current was set to 0.36 pA. This value is in between the extreme values proposed previously (0.07 pA, [36]; 1 pA, [29]), and is close to the experimental estimates of i_{RyR} in planar lipid bilayers under physiological conditions [38,39]. The dyadic calcium release current was thus 17.6 pA, which corresponds to the larger published estimates of Ca release flux [21,25] and was considered the upper limit for a dyad composed of 49 RyRs.

In this study, the dyadic calcium release flux was decreased from this limiting value either by a decrease of the single channel current amplitude or by activating only a subset of RyRs in the dyad during release. A decrease of the calcium current through open RyRs can be considered also as the first approximation of another natural mechanism reducing the ion flux, the rapid flickering of channels. Uncoordinated gating of a subpopulation of channels [41,42] was represented by a decreased surface density of open RyRs in the SR plane. The latter two approaches are extreme cases of very rapid and very slow random openings and closures of RyRs. It can be assumed that realistic RyR kinetics will produce results that are intermediate between these two extremes. Coordinated opening and closure [43] of a subpopulation of channels [19,42] was modeled by a condensed cluster of RyRs in the center of the dyad.

The following processes were taken into account in the model: diffusion of Ca^{2+} and Mg^{2+} ions, of ATP^{2-} and its Ca^{2+} and Mg^{2+} complexes; reactions between ATP^{2-} and Ca^{2+} and Mg^{2+}; and calcium binding by phospholipids of the sarcolemmal membrane, the kinetics of which were modeled using the rapid equilibrium approximation [30,44]. In contrast to the sarcolemma, the calcium binding sites on the SR membrane are not those of phospholipids, but those of the SR calcium pump (SERCA) [31]. It is generally accepted that the SR membrane of the dyadic space is almost completely occupied by the RyRs [6]. Therefore, we have not included any SERCA calcium binding sites on the SR membrane of the dyadic space into the model. The calcium buffers troponin and calmodulin were not included into the dyadic space either. Troponin is present only in the myofilaments. Although calmodulin might be present at a concentration of ~25 μM of Ca^{2+} binding sites [31], this concentration represents only ~10 binding sites per dyad, and simulations that included 0 or 25 μM calmodulin Ca^{2+} binding sites were indistinguishable (data not shown).

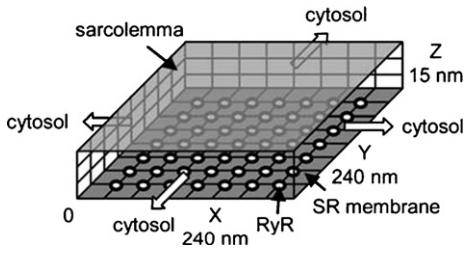

Fig. 1. The model of the dyadic space. The lower and upper planes represent impermeable membranes of the sarcoplasmic reticulum and the sarcolemma, respectively. All side edges are open to cytosol. Circles represent 49 ryanodine receptors modeled as point sources of calcium. The rectangular domain of 240 × 240 × 15 nm (not in scale), representing the dyadic space, was covered by a basic grid of 9 × 9 × 4 nodes.

Table 1
Rate constants of ATP^{2-} reactions

Reaction	Rate constant	Fast set	Slow set
$Ca^{2+}+ATP^{2-}\rightarrow CaATP$	k_1	225 mM^{-1} ms^{-1}	150 mM^{-1} ms^{-1}
$CaATP\rightarrow Ca^{2+}+ATP^{2-}$	k_{-1}	45 ms^{-1}	30 ms^{-1}
$Mg^{2+}+ATP^{2-}\rightarrow MgATP$	k_2	125 mM^{-1} ms^{-1}	1.5 mM^{-1} ms^{-1}
$MgATP\rightarrow Mg^{2+}+ATP^{2-}$	k_{-2}	10.875 ms^{-1}	0.150 ms^{-1}

The fast set of rate constants was taken from [45], while the slow set from [49].

The values of diffusion coefficients were (in $\mu m^2\ s^{-1}$): Ca^{2+}, 300 [46]; Mg^{2+}, 190 [47]; ATP^{2-}, CaATP, and MgATP, 140 [46]. The low- and high-affinity sarcolemmal binding sites had a density of 2.0 and 0.16 $\mu mol\ m^{-2}$, respectively, and half-saturation constants of 1.1 and 0.013 mM, respectively [14].

The rate constants for the reaction of ATP^{2-} with Mg^{2+} under physiological conditions are not known. The published estimates in the literature differ by two orders of magnitude: First, encounter-controlled reaction rates have been assumed, which gave on-rate constants for binding of Mg^{2+} and Ca^{2+} on the same order of magnitude [45], and which are compatible with the results of NMR measurements of MgATP kinetics under less physiological conditions [48]. Second, extrapolations have been made [49] for the on rates based on data measured by the temperature jump method under another conditions [15], which gave on-rate constants for binding of Mg^{2+} and Ca^{2+} differing from each other by two orders of magnitude. Therefore, in the absence of other evidence, we decided to use both sets of rate constants (Table 1) and to compare the results.

In the model, we have neglected the effects of other polyphosphates. Most of them are either present at low concentrations, or their affinity to divalent cations is much less than that of ATP, or both. For instance, the total ADP concentration in the cytosol is ~5μM [45], about three orders of magnitude lower than that of ATP, and the stability of both CaADP and MgADP complexes is approximately 10 times lower than stability of CaATP and MgATP, respectively [45], making the buffering effect of ADP negligible in comparison with ATP.

The initial Ca^{2+} concentration in the dyadic space was set to 0.1 μM, equal to the resting cytosolic concentration. Initial values for other components were calculated from the corresponding chemical equilibria using 3 mM total MgATP concentration, which gave the concentration of both, total ATP and free Mg^{2+} within the range of estimates in a healthy cardiac cell [50–52], and which corresponds to conditions often used in electrophysiological experiments [13,26,28].

Diffusible species such as Ca^{2+}, Mg^{2+}, ATP^{2-}, CaATP, MgATP may diffuse from/into the enclosing cytosolic compartment only at the side edges of the dyadic space, as both the upper and lower boundaries are represented by impermeable membranes. We applied the approximation of a dynamic cytosolic compartment with a volume of 8 μm^3, in which concentrations of all reacting species were considered spatially uniform. However, we considered the temporal dynamics of the chemical reactions in the compartment. The volume of the cytosol was set so that $[Ca^{2+}]$ at the edge of the dyad did not exceed experimentally observed cytosolic calcium levels. In addition to the chemical reactions in the dyadic space, in the cytosolic compartment we also included Ca^{2+} buffering by calmodulin, troponin, and SERCA. Furthermore, we included removal of calcium from the cytosol by SERCA and by the sarcolemmal Na/Ca exchanger (NCX). The parameters of the cytosolic buffers and transport systems were mostly those collected by Stern et al. [18] and they are given in Table 2. The amounts of NCX and SERCA in the cytosolic compartment were adjusted to provide a half-time of calcium decline similar to experimental estimates [53].

2.2. Mathematical description

Assuming diffusion and kinetics to be governed by the Fick's law and the law of mass action, the reaction-diffusion system with an array of n point sources of calcium influx in the dyadic space was described by partial differential equations (PDEs):

$$\frac{\partial[Ca^{2+}]}{\partial t} = D_{Ca}\nabla^2[Ca^{2+}] - k_1[Ca^{2+}][ATP^{2-}] + k_{-1}[CaATP] + \frac{i_{RyR}}{2F}\sum_{i=1}^{n}\delta^3(\mathbf{x}-\mathbf{x}_i) \quad (1a)$$

$$\frac{\partial[Mg^{2+}]}{\partial t} = D_{Mg}\nabla^2[Mg^{2+}] - k_2[Mg^{2+}][ATP^{2-}] + k_{-2}[MgATP] \quad (1b)$$

$$\frac{\partial[CaATP]}{\partial t} = D_{ATP}\nabla^2[CaATP] + k_1[Ca^{2+}][ATP^{2-}] - k_{-1}[CaATP] \quad (1c)$$

$$\frac{\partial[ATP^{2-}]}{\partial t} = D_{ATP}\nabla^2[ATP^{2-}] - k_1[Ca^{2+}][ATP^{2-}] - k_2[Mg^{2+}][ATP^{2-}] + k_{-1}[CaATP] + k_{-2}[MgATP] \quad (1d)$$

$$\frac{\partial[MgATP]}{\partial t} = D_{ATP}\nabla^2[MgATP] + k_2[Mg^{2+}][ATP^{2-}] - k_{-2}[MgATP], \quad (1e)$$

where the symbols in square brackets denote concentrations of reactants at a space location and time t. The symbols ∇^2 and δ^3 stand for the Laplace operator and the Dirac delta function, respectively, both in 3D Cartesian coordinates with the origin set to the left-front-bottom corner of the domain. i_{RyR} represents the unitary Ca^{2+} current of a single RyR channel, F is the Faraday constant and the vectors $\mathbf{x}_i$ describe the space location of the n individual point sources, each carrying the current i_{RyR}. Provided that the diffusion coefficient D_{ATP} is identical for CaATP, MgATP and ATP^{2-}, and provided that the species CaATP, MgATP, and ATP^{2-} were uniformly distributed at time 0, the mass balance equation for the total ATP concentration,

$$c_{ATP} = [CaATP] + [MgATP] + [ATP^{2-}], \quad (2)$$

is fulfilled anywhere in the domain at all times. This means that the summation at the right side of Eq. (2) is invariant in space and time and always equal to c_{ATP}. Hence, [MgATP] in Eqs. (1b) and (1d), as well as the whole PDE for [MgATP] (Eq. (1e)) may be eliminated.

The initial equilibrium values of other components were $[Mg^{2+}]_0$=0.469 mM, $[CaATP]_0$=0.2535 μM, and $[ATP^{2-}]_0$=0.469 mM with the fast set of rate constants (Table 1, [45]). Application of the slow set of rate constants (Table 1, [49]) yielded $[Mg^{2+}]_0$=0.500 mM, $[CaATP]_0$=0.250 μM, and $[ATP^{2-}]_0$=0.500 mM. Impermeability of both membranes for all species was implemented by the boundary condition set for the upper and lower planes. In the case of Ca^{2+}

Table 2
Parameters of the cytosol

Variable description	Unit	Value	Reference
Total calmodulin concentration	mM	0.024	[22]
Total troponin concentration	mM	0.07	[22]
Total SR surface Ca sites	mM	0.047	[22]
Total SL surface Ca sites	mM	1.124	[23]
Calmodulin Ca on rate	mM^{-1} ms^{-1}	100.0	[23]
Calmodulin Ca off rate	ms^{-1}	0.038	[23]
Troponin Ca on rate	mM^{-1} ms^{-1}	39.0	[23]
Troponin Ca off rate	ms^{-1}	0.02	[23]
SR surface Ca on rate	mM^{-1} ms^{-1}	115.0	[23]
SR surface Ca off rate	ms^{-1}	0.1	[23]
SL surface Ca on rate	mM^{-1} ms^{-1}	115.0	[23]
SL surface Ca off rate	ms^{-1}	1.0	[23]
SERCA pump max. rate	mM^{-1} ms^{-1}	5.4×10^{-4}	this work
SERCA pump affinity	mM	3×10^{-4}	[18]
Extracellular calcium	mM	2	[48]
Extracellular sodium	mM	138	[48]
Cytosolic sodium	mM	10	[48]
NCX scaling factor (0 mV)	mM^{-1} ms^{-1}	0.25	this work
Na half-saturation constant for NCX	mM	87.5	[48]
Ca half-saturation constant for NCX	mM	1.38	[48]
NCX saturation factor at negative potentials		0.2	[48]

ions, the boundary condition for the upper plane (sarcolemma) was set as in [54]:

$$\frac{\partial[Ca^{2+}]}{\partial z} = -\frac{1}{D_{Ca}}\left[\frac{N_1K_1}{(K_1+[Ca^{2+}])^2}+\frac{N_2K_2}{(K_2+[Ca^{2+}])^2}\right]\cdot\frac{\partial[Ca^{2+}]}{\partial t}, \quad (3)$$

in accordance with the expression for Ca^{2+} flux density into the cleft from the SL binding sites derived by Langer and Peskoff [30], where N_1, N_2 denote surface densities of low- and high-affinity binding sites, respectively, and where K_1, K_2 are the corresponding half-saturation constants. Time-dependent Dirichlet boundary conditions were prescribed at all four side edges of the dyadic space in conformity with the cytosolic compartment model.

The reaction dynamics in the cytosol was modeled by a set of 8 ordinary differential equations (ODEs), equivalent to Eqs. 4 and 6 of ref. [23], describing the kinetics of Ca^{2+}, Mg^{2+}, CaATP, and ATP^{2-}, and the free forms of the cytosolic calcium buffers calmodulin, troponin, the Ca^{2+} binding sites on the SERCA and those on the SL membranes exposed to cytoplasm. The equations for Ca^{2+}, Mg^{2+}, CaATP, and ATP^{2-} included terms describing fluxes from and into the dyadic space (see the next section for details) and the Ca^{2+} equation included also calcium removal fluxes via SR membrane (J_{SERCA}) and via SL membrane (J_{NCX}), representing SERCA and NCX, respectively. The equations and the respective parameters for description of these fluxes were taken from [18] for J_{SERCA} and from Winslow et al. [55] for J_{NCX} :

$$J_{SERCA} = \frac{V_{max}[Ca^{2+}]_i^2}{K_M^2+[Ca^{2+}]_i^2}, \quad (4)$$

where V_{max} is SERCA pump maximum rate, K_M is SERCA pump affinity (half-saturation constant), and $[Ca^{2+}]_i$ stands for intracellular (cytosolic) free calcium concentration;

$$J_{NCX} = \frac{A\cdot\left(e^{\frac{\eta VF}{RT}}[Na^+]_i^3[Ca^{2+}]_e - e^{\frac{(\eta-1)VF}{RT}}[Na^+]_e^3[Ca^{2+}]_i\right)}{\left(K_{Na}+[Na^+]_e^3\right)\cdot\left(K_{Ca}+[Ca^{2+}]_e\right)\cdot\left(1+e^{\frac{(\eta-1)VF}{RT}}k_{sat}\right)} \quad (5)$$

where the subscripts e and i denote extra- and intracellular concentrations of ions, respectively, A represents a scaling factor of Na/Ca exchange, K_{Na} and K_{Ca} are Na^+ and Ca^{2+} half saturation constants for Na/Ca exchange, respectively, k_{sat} denotes Na/Ca exchange saturation factor at negative potentials, η=0.35 characterizes the voltage dependence of NCX, and V=0 mV except when specifically noted otherwise. The parameters are summarized in Table 1 and Table 2. The initial equilibrium concentrations in the model of the cytosol were the same as those in the model of the dyadic space.

2.3. Numerical methods and software

For solving the set of time-dependent PDEs (Eq. (1)) we used a Vectorizable Local Uniform Grid Refinement (VLUGR3) solver for PDEs in 3D [56,57], as described previously [54]. In brief, the solver is coded in Fortran77 and it uses the Method of Lines combining an implicit time-stepping method with the adaptive grid algorithm. For space discretization, standard second-order differences are used. Where grid refinement is required, a grid cell is divided into 8 equal parts. The resulting system of ODEs or differential-algebraic equations (DAEs) is solved in time with the second-order two-step implicit BDF (backward differentiation formula) method with variable step sizes.

The domain representing the dyadic space (Fig. 1) was covered by a basic grid of 8×8×3 elements. The maximal grid refinement was restricted to level 3. The maximum number of grid nodes was then 324, 2023, and 14157 at the levels 1, 2, and 3, respectively. The smallest space element was 7.5×7.5×1.25 nm. The system of ODEs modeling the reaction kinetics in the cytosol surrounding the dyadic space was solved simultaneously with the PDEs modeling the reaction-diffusion kinetics inside the domain, using the routine LSODE from the Fortran77 package ODEPACK [58]. ODEs were solved for each time interval between two successive time steps generated by the PDEs solver (VLUGR3). The fluxes from/into the domain were calculated from normal gradients of all components at the side edges of the domain, and were taken as constant during a single time interval. After each VLUGR3 time step, the cytosolic concentrations and the flux magnitudes were updated and used to evaluate the Dirichlet boundary conditions at the actual time in the next step. The LSODE solution was returned exactly at the desired time. To simulate behavior of the model during the relaxation period after closure of the RyR channels, the solver was restarted with the initial conditions set to the values calculated at the time of closure.

Due to the rectangular symmetry of the dyadic space in xy planes, the calculation space could have been reduced to a single quadrant of the whole area. Nevertheless, as the dyadic model was not generally intended to be symmetric, we decided to perform calculations in the full space. A typical simulation required 101 time steps for the first period (10 ms) when all RyRs were open, using the initial time step DT=3 ns. The second relaxation period (from 10 ms to 10 s) took additional 80 time steps with the initial DT=0.1 μs. The simulated data were visualized and calculations were performed in Origin (Ver. 7SR4, OriginLab, Northampton, MA) using LabTalk and OriginC.

2.4. Computer simulations

Computations were carried out on a PC i686 equipped with a 1.84 GHz AMD Athlon XP 2500+processor and 1 GB RAM memory operating under Red Hat Linux 2.4.20–8. The g77 compiler at O2 optimization level was used. Computing time varied from ~4 min to ~1 h depending on the number of active channels and the magnitude of unitary current.

To test the accuracy of our mathematical implementation of the model, the physical time of the simulation was increased to 5 s while simultaneously turning the pump fluxes off. This time was long enough to ensure equilibration of all system components after closure of channels at t=10 ms. The final concentrations were then used to verify the mass balance of calcium with respect to the amount of Ca^{2+} ions that entered the dyadic space and the surrounding cytoplasmic area. The mass balances of Mg^{2+} and ATP^{2-} were also verified by comparing final concentrations of $[ATP^{2-}]+[CaATP]$ to $[Mg^{2+}]$. In addition, all equilibrium constants were recalculated using the final concentrations and compared to those determined from the input rate constants. The relative error did not exceed 3.5% in any case. Calcium mass balance was examined also at each VLUGR3 time step by comparison of the total initial amount of calcium updated by the total calcium influx from the SR at the current time with total calcium at the given moment (cytosolic pumps were turned off). The relative error did not exceed 1% in this case.

3. Results

The purpose of the simulation was to determine the dynamics of free Ca^{2+} concentration in the dyadic space during calcium release with consideration of the major chemical species known to participate in calcium binding. Therefore, we have simulated the time course of Ca^{2+}, Mg^{2+}, and ATP diffusion and binding in the model dyad (Fig. 1) to assess their possible modulatory effect on RyR gating and on the dynamics of calcium release activation and termination.

3.1. Spatiotemporal evolution of Ca^{2+}, Mg^{2+} and ATP^{2-} concentration profiles

The distribution and evolution of Ca^{2+}, Mg^{2+}, and ATP^{2-} concentrations differed significantly. In the case of Ca^{2+}, in addition to the overall gradient that developed over the dyadic space, steep local gradients persisted near each RyR (Fig. 2A and D). The steady state was reached in two steps. During the early phase, the free Ca^{2+} increase was similar above both, the central and the peripheral RyR (Fig. 2G). Due to calcium binding to the high-affinity sarcolemmal binding sites, a pseudo-steady state leveled off at ~300 μM between 0.1 and 100 μs. After that, the free calcium level started to rise,

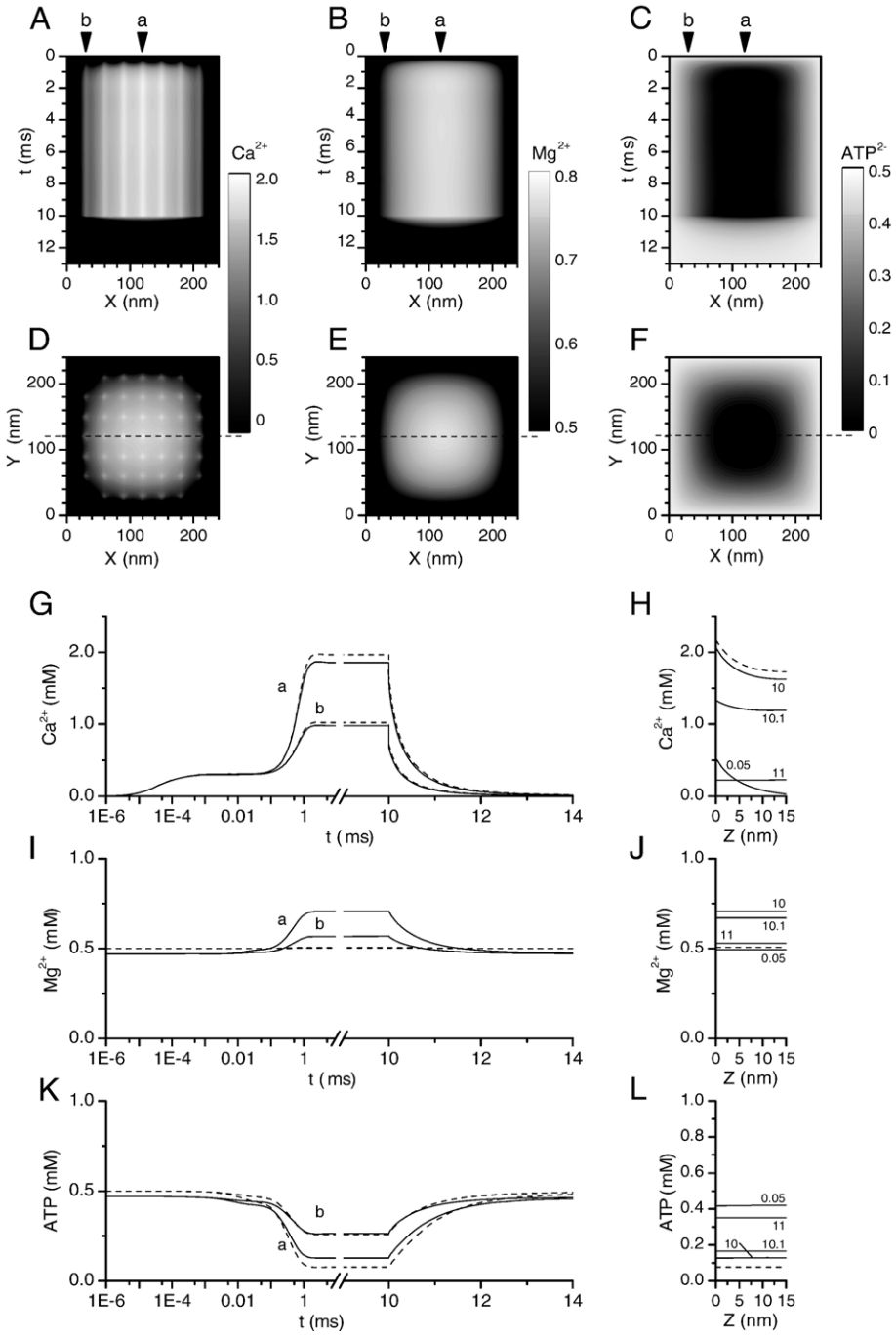

Fig. 2. Spatial distribution and temporal evolution of Ca^{2+}, Mg^{2+}, and ATP^{2-} in the dyadic space. Panels A–C show the respective temporal evolution of Ca^{2+}, Mg^{2+}, and ATP^{2-} concentration across the dyad along the reference line 2.5 nm above the SR membrane at $Y=120$ nm (dashed lines in panels D, E, F). Panels D, E, F show steady state concentration of Ca^{2+}, Mg^{2+}, ATP^{2-}, respectively, in the reference plane 2.5 nm above the SR membrane 10 ms after start of calcium release. Panels G, I, K show the time course of Ca^{2+}, Mg^{2+}, ATP^{2-} concentrations, respectively, at the reference point above the central (a) and outermost (b) RyRs (arrows in panels A–C). Panels H, J, L show the spatial profiles of Ca^{2+}, Mg^{2+}, ATP^{2-} concentrations, respectively, along the Z-axis in the center of the dyad ($X=Y=120$ nm) at different times (shown next to the traces in ms) from the start of calcium release. Solid lines represent simulations with the fast set of rate constants; dotted lines represent simulations with the slow set of rate constants (Table 1).

increasing more steeply in the center than at the edge of the dyadic space. The half-maximal levels were reached within 0.5 ms at both positions. The final steady state above the central (1.8 mM) and the peripheral RyR (1.0 mM) was also achieved simultaneously at ~2 ms (Fig. 2G). At this time, spatially averaged free Ca^{2+} concentration in the dyadic space amounted to 0.70 mM. The fixed buffers did not affect the ultimate level of Ca^{2+} concentration.

Calcium release was accompanied by a sizable increase in Mg^{2+} (Fig. 2B, E, and I) and decrease in ATP^{2-} concentrations (Fig. 2C, F, and K) when the fast set of rate constants for reactions of ATP^{2-} with Ca^{2+} and Mg^{2+} was used (Fig. 2, solid

lines). Using the slow set of rate constants [49] (Fig. 2, dashed lines) instead of the fast set did not affect spatiotemporal profiles for Ca^{2+} substantially, but it had a strong effect on both, Mg^{2+} and ATP^{2-} profiles. The amplitude of concentration changes of Mg^{2+} evoked by calcium release was strongly decreased, while the amplitude of concentration changes of free ATP^{2-} was increased appreciably. Steady state spatial distribution of both Mg^{2+} and ATP^{2-} did not track local Ca^{2+} inhomogeneities in the dyadic space, because Ca/Mg/ATP complexation kinetics was delayed after Ca^{2+} diffusion from the sources. Therefore, Mg^{2+} and ATP^{2-} concentrations displayed a single global extreme in the center of the dyadic space.

After termination of calcium release, concentrations of Ca^{2+}, Mg^{2+}, and ATP^{2-} returned rapidly back with half-times of 0.25 ms, 0.4 ms, and 0.6 ms for Ca^{2+}, Mg^{2+} and ATP^{2-}, respectively. This rapid component of equilibration proceeded until the concentration of the given species in the dyadic space and in the cytosol was almost the same (within ~40 ms). At this time, the free Ca^{2+} concentration in the cytosol was 0.5 μM. After that, the equilibration of species in the dyadic space and in the cytosol proceeded at the same rate (see below).

The calculations of Ca^{2+}, Mg^{2+}, and ATP^{2-} concentrations along the Z-axis, i.e., between the membranes of the dyadic cleft (Fig. 2H, J, and L) also revealed substantial differences between distribution of Ca^{2+} and of Mg^{2+} and ATP^{2-}. Concentration gradient of Ca^{2+} along the Z-axis at the central RyR built up within 50 μs, reached ~0.4 mM/15 nm in the steady state, and briskly dissipated after termination of calcium release. Nevertheless, the distribution of Mg^{2+} (Fig. 2J) and ATP^{2-} (Fig. 2L) along the Z-axis was homogenous due to spatiotemporal buffering.

The maximal Mg^{2+} concentration within the dyadic space achieved during calcium release, calculated using the fast set of rate constants, was 0.71 mM (Fig. 2I and J), i.e., by approximately 50% higher than the resting level. At the same time, concentration of ATP^{2-} was significantly reduced from 0.47 mM to 0.13 mM in the center of the dyadic space. The decrease of free ATP^{2-} was even more profound with the slow set of rate constants, from 0.50 mM to 0.076 mM.

3.2. The effect of diffusion coefficients on concentration profiles in the dyadic space

The effect of diffusion coefficients on the profiles of free Ca^{2+}, Mg^{2+} and ATP^{2-} concentrations is documented in Fig. 3A–C. It can be seen (Fig. 3A) that using the highest diffusion coefficients still led to a substantial accumulation of Ca^{2+} in the dyadic space. On the other hand, the related changes in free ATP^{2-} concentration were substantially attenuated at elevated diffusion coefficients (Fig. 3C) and the changes in free Mg^{2+} concentration (with the fast set of rate constants) were almost obliterated (Fig. 3B). Reduction of diffusion coefficients to the lowest estimates resulted in massive accumulation of Ca^{2+} (Fig. 3A) and Mg^{2+} (with the fast set of rate constants; Fig. 3B) and to substantial reduction of ATP^{2-} (Fig. 3C). The use of the slow set of rate constants (Fig. 3, dashed lines) led to similar profiles of steady state Ca^{2+} distribution, but the concentration of Mg^{2+} remained almost unaffected and changes in free ATP^{2-} concentration displayed a more pronounced trend, resulting in virtual elimination of ATP^{2-} from the central region of the dyadic space at low diffusion coefficients.

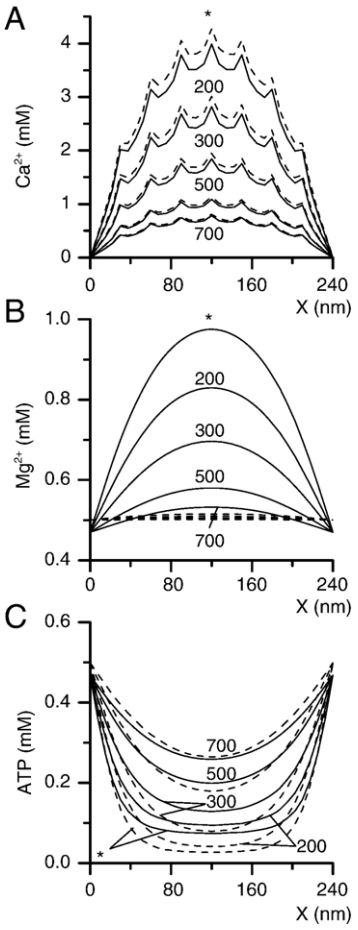

Fig. 3. Steady state concentration profiles of Ca^{2+} (A), Mg^{2+} (B), ATP^{2-} (C) across the dyadic space for various diffusion coefficients. Y=120 nm, Z=2.5 nm, t=10 ms. The labels at individual traces denote values of D_{Ca} (in units of $\mu m^2\ s^{-1}$) used in calculations. The values of D_{Ca} were the same in all spatial directions, except for the traces labeled with an asterisk (*), which were calculated using D_{Ca} values of 140, 140, 350 $\mu m^2\ s^{-1}$ for the X, Y and Z direction, respectively [31]. Solid lines represent simulations with the fast set of rate constants; dotted lines represent simulations with the slow set of rate constants (Table 1).

3.3. The effect of Ca^{2+} release current on concentration changes in the dyadic space

The spatiotemporal dynamics of ion concentrations in the dyadic space during calcium release is determined mainly by the dyadic calcium release current (i_{CRU}), given by the number of RyRs (n_{RyR}) and their single-channel amplitude (i_{RyR}).

To get insight into the effect of the single channel current amplitude and of the open RyR channel density on the spatiotemporal dynamics, we have varied the i_{CRU} in three different ways. In the first approach, the single-channel amplitude of current flowing through each of the 49 RyRs was varied. In the second approach, a cluster of neighboring RyRs containing a

variable number of channels that carry the release current was positioned in the center of the SR membrane (see the top center panel of Fig. 4). In the third approach, the surface density of open RyRs was varied (see the top right panel of Fig. 4). Whereas reduction of the single-channel amplitude of RyRs led to a homogenous decrease of the spatial density of Ca^{2+} release flux, decreasing the size of the RyR cluster reduced the spatial density of Ca^{2+} release flux predominantly in the peripheral areas of the SR plane. The third approach provided intermediate changes of spatial density of Ca^{2+} flux.

The effect of dyadic calcium release current on the time course of concentration changes of Ca^{2+}, Mg^{2+}, and ATP^{2-} in the dyadic space was analyzed using simulations analogous to those of Fig. 2. All three model types showed two phases of Ca^{2+} and Mg^{2+} increase and ATP^{2-} decrease. After an early increase of Ca^{2+} concentration, a transient pseudo-stationary phase developed and persisted for ~100 μs, during which calcium influx into the dyadic space was temporarily buffered by the sarcolemmal calcium binding sites (Fig. 4B). At these times, only fixed calcium buffers in the immediate vicinity of RyR channels became significantly saturated by Ca^{2+}. Therefore, as demonstrated in Fig. 4A, the increase in Ca^{2+} concentration above any channel was proportional to the amplitude of calcium current flowing through the channel itself and was not significantly affected by calcium flux through neighboring channels. For the same reason, models in which n_{RyR} was varied showed almost no effect of i_{CRU} on the resulting Ca^{2+} concentration above individual RyRs. At these early times, almost no change in the concentration of Mg^{2+} could be observed, while concentration of ATP^{2-} at the reference point was decreased by up to ~10% from the basal value, and the amplitude of its change was approximately proportional to i_{CRU}. Using the slow set of rate constants provided almost the same linear dependence of Ca^{2+} concentration on i_{RyR} but no change in Mg^{2+} concentration with increasing i_{CRU}. The free ATP^{2-} was affected to a similar extent as for the fast set of rate constants.

Saturation of the sarcolemmal Ca^{2+} binding sites during prolonged calcium release led to a large increase of calcium concentration in the dyadic space and to formation of a new steady state within 1 to 3 ms, depending on the amplitude of i_{CRU} as well as on the arrangement of open RyRs in the dyad (Fig. 4B). This time, Ca^{2+} increase was closely followed by a substantial increase in the concentration of Mg^{2+} (with the fast set of rate constants; Fig. 4C) and by a substantial decrease of ATP^{2-} concentration (Fig. 4D).

The calculated steady-state spatial profiles of Ca^{2+}, Mg^{2+}, and ATP^{2-} are provided in Fig. 4E, F, and G, respectively, for different i_{CRU} values. Due to fast saturation of a significant fraction of calcium buffers in the whole volume of the dyadic space (data not shown), higher spatial density of dyadic Ca^{2+} release flux led to higher increases in both, Ca^{2+} and Mg^{2+}, and to a stronger decrease in ATP^{2-}. Models where the value of i_{RyR} was varied showed a linear dependence between i_{CRU} and Ca^{2+}, Mg^{2+}, and ATP^{2-} concentration change (left panels of Fig. 4E–G). In contrast, in models with varied size of clusters (center panels of Fig. 4E–G), the amplitudes of changes in steady-state concentrations of Ca^{2+}, Mg^{2+}, and ATP^{2-} steeply increased as the number of RyRs in the condensed cluster rose from one to 5, but they were similar when n_{RyR} was increased from 25 to 49. Activation of a cluster of RyRs in the center of the SR membrane plane (Fig. 4E, center panel) produced much higher peak calcium levels than activation of RyRs evenly distributed over the SR membrane plane (Fig. 4E, right panel). The effect of channel surface density on Ca^{2+}, Mg^{2+}, and ATP^{2-} concentrations (right panels of Fig. 4E–G) was similar by extent to the effect of single-channel amplitude (left panels of Fig. 4E–G), but differed somewhat in spatial distribution due to different coordinates at which a RyR channel was present.

Calculations using the slow set of rate constants (Table 1) provided a negligible difference in Ca^{2+} concentration profiles (Fig. 4E). Importantly, they provided almost no accumulation of Mg^{2+} ions within the dyadic space (Fig. 4F). At the same time, however, combination of free ATP^{2-} with the released Ca^{2+} was significantly larger than for the fast set of rate constants (Fig. 4G), obviously due to negligible participation of Mg^{2+} ions in the reaction in the system.

Distribution of the Ca^{2+} release sources over the SR plane had little effect on the changes of steady-state concentrations of Ca^{2+}, Mg^{2+}, and ATP^{2-} averaged over the whole volume of the dyadic space, which were approximately proportional to the calcium release current. Decreasing the size of the central cluster of RyRs was slightly less effective than decreasing the single-channel amplitude or the RyR surface density in decreasing the concentration changes induced by the release current.

3.4. Time course and amplitude of concentration changes in the cytosol

For the basic model, free calcium in the cytosol increased to ~0.83 μM during 10 ms of calcium release (Fig. 5A). Under these conditions, CaATP reached a peak concentration of 2.0 μM with the fast set of rate constants (Fig. 5B) and 2.1 μM with the slow set (data not shown). The cytosolic values of free Mg^{2+} and MgATP concentrations were practically unchanged, as expected for such a small change of Ca^{2+}. If the calcium release flux was decreased, the cytosolic increase in free Ca^{2+} and CaATP was almost proportionally reduced. The time course of Ca^{2+} and CaATP in the cytosol did not depend measurably on the model of calcium release, i.e., it was the same whether i_{CRU} was changed by changing i_{RyR} or cluster size. It was also independent of the diffusion coefficients in the dyadic space and of the rate constants of reactions between ATP^{2-} and the Ca^{2+} and Mg^{2+} ions. After release termination, the majority of Ca^{2+} was extruded from the cytosol by the action of SERCA and a smaller fraction was extruded by NCX. For the parameters given in Table 2, this process could be approximated by two exponential components. About 30% of Ca^{2+} decreased with a time constant of 15 ms, whereas the remaining ~70% decreased with a time constant of 230 ms. We suppose that the time course of Ca^{2+} decline is based on the Michaelis–Menten kinetics of SERCA, coupled with the kinetics of cytosolic buffering.

For the given set of parameters, the size of the cytosolic compartment (in the range of 1–10000 μm^3) had negligible

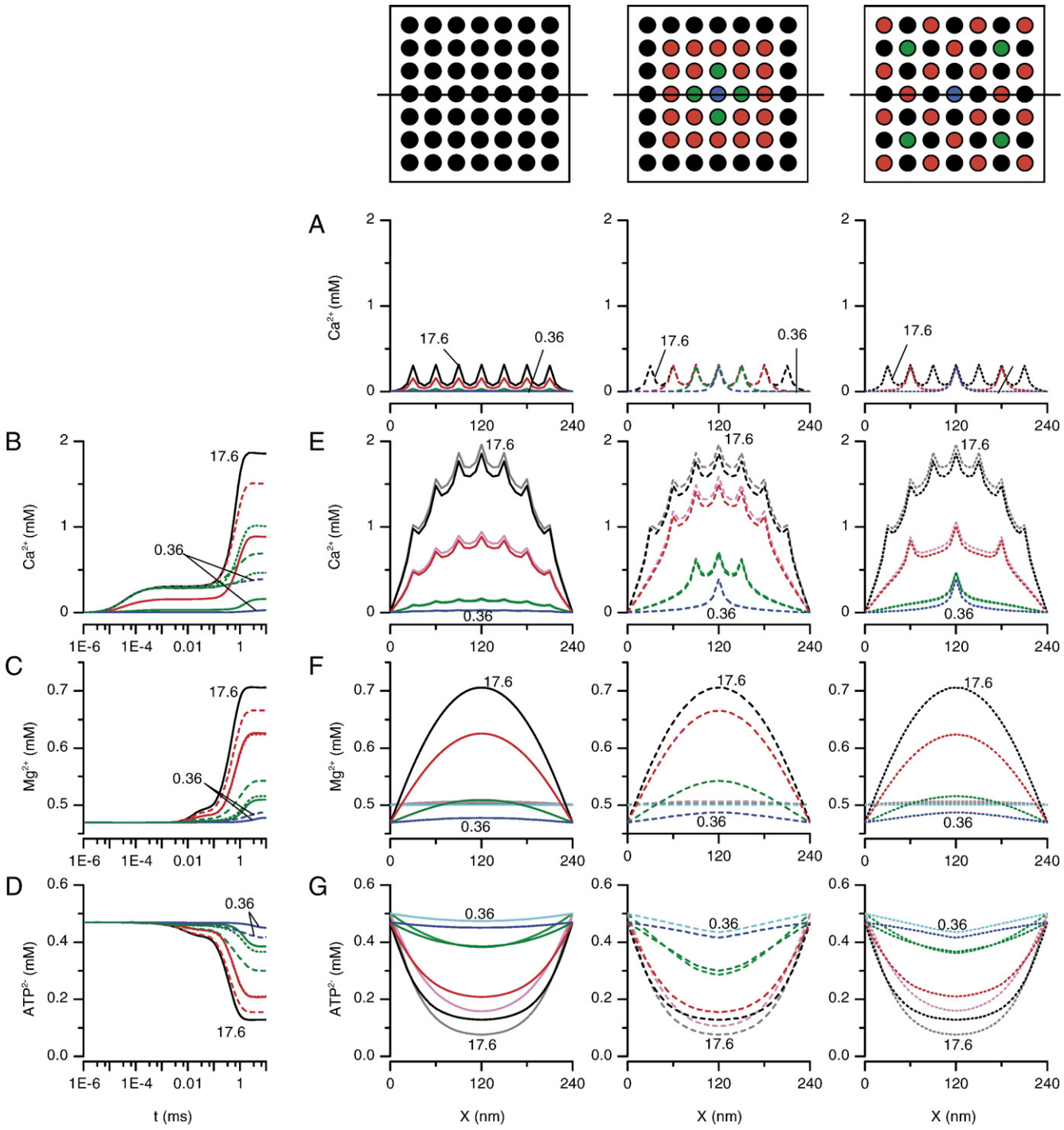

Fig. 4. Steady state concentration profiles across the dyadic space for various values of dyadic calcium release current (i_{CRU}). Top panels show the geometry of RyR clusters (blue, green, red and black circles for 1, 5, 25 and 49 RyRs, respectively). Panel A shows the calcium concentration profiles 100 μ after start of calcium release for various i_{CRU} values, resulting from variation of the unitary current amplitude of RyRs (left panel), of the number of open RyRs clustered at the center of the SR membrane (center panel), of the number of open RyRs distributed across the SR membrane (right panel), respectively. Panels B, C, D show the time course of Ca^{2+}, Mg^{2+}, ATP^{2-}, respectively, at the reference point, corresponding to the center of the top panels, for various i_{CRU} values and for the fast set of rate constants. Panels E, F, G show the steady-state concentration profiles of Ca^{2+}, Mg^{2+}, ATP^{2-}, respectively for various i_{CRU} values, resulting from variation of the unitary current amplitude of RyRs (left panels), of the number of open RyRs clustered at the center of the SR membrane (center panels), of the number of open RyRs distributed across the SR membrane (right panels), respectively. Dyadic calcium release current ($i_{CRU}=i_{RyR}\times n_{RyR}$) was 17.6, 9.0, 1.80, 0.36 pA; the largest and the smallest values of i_{CRU} are given next to the traces). Black, red, dark green and dark blue lines represent simulations with the fast set of rate constants; grey, pink, light green and cyan lines represent simulations with the slow set of rate constants (Table 1). Solid, dashed and dotted lines represent simulations with variable single channel amplitude, cluster size, RyR density, respectively.

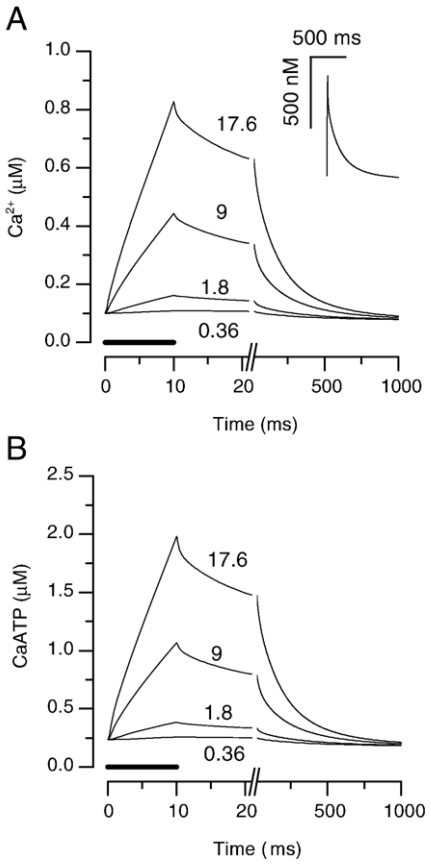

Fig. 5. Time course of Ca^{2+} (A) and CaATP (B) concentrations in the cytosol for various dyadic calcium release currents. The duration of release (10 ms) is marked by the thick line. Labels next to the traces denote values of the dyadic calcium release current in units of pA. In the inset, cytosolic calcium transient in response to the standard calcium release current (i_{CRU} =17.6 pA) is shown on a linear scale.

impact (<5%) on the time course and spatial profile of any species in the center of the dyadic space during calcium release (data not shown). At the edge of the dyadic space, where concentrations of all reactants were equal to their cytosolic concentrations, the concentration of free Ca^{2+} decreased with increasing volume of the cytosol (not shown).

4. Discussion

Calcium release in the cardiac dyad as a reaction-diffusion problem was previously analyzed only in a one-dimensional approximation [14,30]. In the presented model, the dyadic space was defined in all three spatial dimensions, and Mg^{2+} and ATP^{2-} were added to the system. Simulations revealed substantial spatial variation of both, the instantaneous and the steady state Ca^{2+} concentrations, in the vicinity of RyRs. This result indicates that very local Ca^{2+} control, at the scale of nanometers, should be considered in E–C coupling phenomena. Additionally, 3D modeling revealed that during a typical open time of RyRs, ~2 ms in the H-mode [18,10,17,59], local Ca^{2+} concentration can exceed 1 mM. This high local concentration of Ca^{2+} asks for consideration of the role of Ca^{2+} dependent inactivation of RyRs in termination of Ca^{2+} release. Short open times of RyRs, such as those of the L-mode [59], lasting for few hundred microseconds or less, may provide Ca levels of only ~300 μM, due to the buffering effect of plasmalemmal Ca binding sites (Fig. 2G).

Inclusion of Mg^{2+} and ATP^{2-} into calculations was also productive despite their lower spatial dynamics. The concentration profile of Mg^{2+} strongly depended on the kinetics of its complexation with ATP^{2-}. With the fast set of rate constants [45], the increase of Mg^{2+} concentration by up to 50% led to steady-state values effectively inhibiting RyR open probability in bilayer experiments [10–12]. Importantly, Mg^{2+} has been shown to act not only as a competitive inhibitor of Ca^{2+}-induced activation [10–12,16], but also at a separate inhibitory site [11,12], where its apparent IC_{50} value has been determined to be ~10 mM at a constant calcium concentration [11] but as low as ~0.7 mM immediately after activation by high Ca^{2+} concentrations [12]. Therefore, although in the steady state, modulation of the channel by Mg^{2+} exerts only a modest effect on RyR open probability [16], its effect upon rapid activation of RyRs may be much more prominent. In contrast, with the slow set of rate constants [49], Mg^{2+} concentrations changed by less than 5% and therefore under these conditions Mg^{2+} would not be expected to exert a dynamic effect on RyR open probability.

The concentration of ATP^{2-} inside the dyadic space decreased substantially during Ca release. The effect was pronounced for both sets of rate constants because the kinetics of CaATP formation was sufficiently fast in both cases. Free ATP^{2-} concentration was decreased down to 0.1 mM, that is, to levels below the EC_{50} for RyR activation [17]. Additionally, even if the decrease of ATP does not lead to a drastic decline of open probability, it potentiates the inhibitory effect of Mg^{2+} [16].

At present the lack of quantitative models of RyR modulation by Ca^{2+}, Mg^{2+} and ATP^{2-} precludes predicting the effect of changes in concentrations of these ions on RyR activity during release quantitatively. However, taken together, the increase of free Ca^{2+} to the millimolar range, accompanied by a decrease of free ATP^{2-} below 200 μM, and eventually by an increase of free Mg^{2+} above 0.7 mM, might contribute substantially to reduction of the RyR open probability and thereby to cessation of Ca release. In other words, our calculations indicate that under physiological conditions the termination of Ca release may result from the synergic effect of the construction and chemistry of the mammalian cardiac dyad. The importance of this effect will increase with increasing dyadic calcium release current (Fig. 4) and decreasing diffusion coefficient (Fig. 3).

An interesting outcome of the modeling is the finding that within a millisecond, Ca^{2+} concentration in the center of the dyadic space becomes comparable to the free calcium level in the SR lumen at calcium loads generally considered to be normal ~1 mM [50]. In this context it is notable that higher free Ca levels of up to 2 mM were reported by Shannon et al. [60]. Nevertheless, our simulations show that if the calcium flux in a single calcium release unit is as high as reported

[21,24–27,29], the concentration gradient of Ca^{2+} ions between the lumen of the terminal cistern and the dyadic space may vanish. This may happen even when the number, planar density, or conductance of RyRs is at their low margin (Fig. 4) or if the Ca^{2+} diffusion coefficient is at its high margin (Fig. 3). We suggest that the most effective value of i_{CRU} is that producing a steady state level of [Ca^{2+}] in the cleft close to the luminal concentration. Although the calcium gradient across the SR membrane vanishes almost to zero in that case, this may not inevitably lead to a substantial decrease of the calcium flux, as the driving calcium gradient is then shifted towards the boundary of the dyadic space with the cytosol. That is, although Ca^{2+} concentration at certain locations within the dyad approaches luminal concentration, the cytosolic Ca concentration remains low and rises very slowly, and the overall driving force acting on Ca ions in the SR lumen stays very high during the period simulated in this study. Thus, an appropriate number of optimally operating RyRs in the dyad should not represent a hindrance to calcium flux and the bottleneck of the whole Ca release process (driven by the difference between the Ca^{2+} chemical potential of the SR lumen and of the cytosol) will be the geometry of the dyadic junction. This means that increasing the number of open RyRs will not substantially increase the calcium release flux, because release will be limited by the radial diffusional resistance of the dyadic space (in contrast to skeletal dyads/triads). This effect might be of importance for the relation between the SR calcium load and calcium release flux, i.e., for E–C coupling efficiency.

4.1. Spatiotemporal distribution of Mg^{2+} and ATP^{2-} within the dyadic space

The spatiotemporal distribution of Mg^{2+} and ATP^{2-} was strongly dependent on the rate constants for formation and dissociation of the MgATP complex.

The fast set of rate constants (Table 1, [45]) is based on the near-diffusion-limited value for the on-rate constant of Mg^{2+} binding to ATP^{2-}. Its use results in a sizeable transient decline of free ATP^{2-} accompanied with a substantial elevation of [Mg^{2+}] in the dyadic space during calcium release. On the other hand, the slow set of rate constants [49] was extrapolated from the values obtained by Eigen and Wilkins [15] under conditions very different from the physiological conditions. Its use results in a more profound transient decline of free ATP^{2-} and a negligible elevation of [Mg^{2+}] in the dyadic space during calcium release. To resolve these uncertainties, the rate constants in question should be measured with higher precision under conditions mimicking the cellular environment.

4.2. Limitations of the present study

There are several methodological limitations in this study. We used an approximation of constant i_{RyR} during the whole period of calcium release to estimate an upper limit of Ca^{2+} concentration in the dyadic space and its effect on the other species subsequently produced or consumed (Mg^{2+}, ATP^{2-}). The unitary RyR current may be time-dependent due to local depletion of Ca^{2+} in the junctional SR [61,62] that may lead to a reduction of the calcium gradient across the SR membrane. However, calcium release fluxes determined experimentally [29] suggested a constant single-channel current through RyRs that was independent of the calcium release flux during simultaneous opening of 1 to 7 RyRs in a spark. Kubalova et al. [61] provided calibrated records (their Fig. 5B and Fig. 4C), from which it can be estimated that the extent of luminal Ca depletion is not substantial: the free luminal Ca decreased only by 15% within 50 ms from the commencement of calcium release.

We have simulated calcium release without the inclusion of calcium influx through the DHPR channels, approximating a spontaneous dyadic calcium release event. Calcium influx through a DHPR channel would pre-elevate Ca^{2+} concentration in the dyadic space to ~70 μM [31], and therefore the temporal Ca^{2+} profile during triggered calcium release event would differ from our simulations during the first few microseconds of calcium release (cf. Fig. 2G).

Due to the stochastic nature of RyR gating, the number of activated RyRs and the number of simultaneously open RyRs in the cluster may be limited to only a fraction of channels in the terminal cistern. Indeed, confocal experiments on rat cardiac myocytes [21,26,29,41] suggest that the number of simultaneously open RyRs during a calcium spark is substantially lower than electron-microscopic estimates of the total RyR number per dyad [6]. As illustrated in Fig. 4, the number, surface distribution, and mean open time of RyRs are important for Ca^{2+} accumulation in the dyadic space. Therefore, inclusion of stochastic activity of RyRs, according to an appropriate gating model, would be useful for exact description of both Ca^{2+} dynamics and the coupled Mg^{2+} and ATP^{2-} dynamics.

We have used the continuous approximation for simulation of the dyadic space, although the total number of interacting particles in the dyad is relatively low. The resulting picture should be therefore seen as an average dyad of a typical myocyte or as the average of many release events, as previously proposed [20]. Nevertheless, we assume that the errors introduced by the continuum approximation will be smaller than the inaccuracies introduced by the uncertainties in the model parameters.

In the present version of our model, we have not included electrodiffusion. Its effects on the calcium profiles in the case of Ca^{2+} release should be smaller than those in the case of Ca^{2+} influx through the sarcolemma [31], because the Ca^{2+} sources are located at the SR membrane, supposedly free of surface charges. Therefore the concentrations of ions near the RyRs, which are >10 Debye lengths from the sarcolemmal surface charges, will be only slightly affected.

Acknowledgements

This work was supported by grants 1/0068/03 from Vedecká Grantová Agentúra and 51-031104 from Agentúra na podporu výskumu a vývoja, and by the National Institutes of Health

Fogarty International Research Collaboration Award R03 TW05543 to Sándor Györke. The research of A. Zahradníková was supported in part by a Howard Hughes Medical Institute International Scholar's Award.

References

[1] H. Cheng, W.J. Lederer, M.B. Cannell, Calcium sparks: elementary events underlying excitation–contraction coupling in heart muscle, Science 262 (1993) 740–744.

[2] M.B. Cannell, H. Cheng, W.J. Lederer, Spatial non-uniformities in $[Ca^{2+}]_i$ during excitation–contraction coupling in cardiac myocytes, Biophys. J. 67 (1994) 1942–1956.

[3] J.R. Lopez-Lopez, P.S. Shacklock, C.W. Balke, W.G. Wier, Local calcium transients triggered by single L-type calcium channel currents in cardiac cells, Science 268 (1995) 1042–1045.

[4] M.B. Cannell, H. Cheng, W.J. Lederer, The control of calcium release in heart muscle, Science 268 (1995) 1045–1049.

[5] M. Radermacher, V. Rao, R. Grassucci, J. Frank, A.P. Timerman, S. Fleischer, T. Wagenknecht, Cryo-electron microscopy and three-dimensional reconstruction of the calcium release channel/ryanodine receptor from skeletal muscle, J. Cell Biol. 127 (1994) 411–423.

[6] C. Franzini-Armstrong, F. Protasi, V. Ramesh, Shape, size, distribution of Ca(2+) release units and couplons in skeletal and cardiac muscles, Biophys. J. 77 (1999) 1528–1539.

[7] L.F. Santana, H. Cheng, A.M. Gomez, M.B. Cannell, W.J. Lederer, Relation between the sarcolemmal Ca^{2+} current and Ca^{2+} sparks and local control theories for cardiac excitation–contraction coupling, Circ. Res. 78 (1998) 166–171.

[8] A. Zahradníková, I. Zahradník, I. Györke, S. Györke, Rapid activation of the cardiac ryanodine receptor by submillisecond calcium stimuli, J. Gen. Physiol. 114 (1999) 787–798.

[9] G. Meissner, Ryanodine receptor/Ca^{2+} release channels and their regulation by endogenous effectors, Annu. Rev. Physiol. 56 (1994) 485–508.

[10] I. Györke, S. Györke, Regulation of the cardiac ryanodine receptor channel by luminal Ca^{2+} involves luminal Ca^{2+} sensing sites, Biophys. J. 75 (1998) 2801–2810.

[11] D.R. Laver, T.M. Baynes, A.F. Dulhunty, Magnesium inhibition of ryanodine-receptor calcium channels: evidence for two independent mechanisms, J. Membr. Biol. 156 (1997) 213–229.

[12] A. Zahradníková, M. Dura, I. Györke, A.L. Escobar, I. Zahradník, S. Györke, Regulation of dynamic behavior of cardiac ryanodine receptor by Mg2+ under simulated physiological conditions, Am. J. Physiol.: Cell Physiol. 285 (2003) C1059–C1070.

[13] A. Zahradníková, Z. Kubalová, J. Pavelková, S. Györke, I. Zahradník, Activation of calcium release assessed by calcium release-induced inactivation of calcium current in rat cardiac myocytes, Am. J. Physiol.: Cell Physiol. 286 (2004) C330–C341.

[14] A. Peskoff, J.A. Post, G.A. Langer, Sarcolemmal calcium binding sites in heart: II. Mathematical model for diffusion of calcium released from the sarcoplasmic reticulum into the diadic region, J. Membr. Biol. 129 (1992) 59–69.

[15] M. Eigen, R.G. Wilkins, The kinetics and mechanism of formation of metal complexes, Adv. Chem. Ser. 49 (1965) 55–67.

[16] L. Xu, G. Mann, G. Meissner, Regulation of cardiac Ca^{2+} release channel (ryanodine receptor) by Ca^{2+}, H^+, Mg^{2+}, adenine nucleotides under normal and simulated ischemic conditions, Circ. Res. 79 (1996) 1100–1109.

[17] H. Kermode, A.J. Williams, R. Sitsapesan, The interactions of ATP, ADP, inorganic phosphate with the sheep cardiac ryanodine receptor, Biophys. J. 74 (1998) 1296–1304.

[18] M.D. Stern, L.S. Song, H. Cheng, J.S. Sham, H.T. Yang, K.R. Boheler, E. Rios, Local control models of cardiac excitation–contraction coupling. A possible role for allosteric interactions between ryanodine receptors, J. Gen. Physiol. 113 (1999) 469–489.

[19] H. Cheng, Putting out the fire: what terminates calcium-induced calcium release in cardiac muscle? Cell Calcium 35 (2004) 591–601.

[20] C. Soeller, M.B. Cannell, Analysing cardiac excitation–contraction coupling with mathematical models of local control, Prog. Biophys. Mol. Biol. 85 (2004) 141–162.

[21] J.H. Bridge, P.R. Ershler, M.B. Cannell, Properties of Ca^{2+} sparks evoked by action potentials in mouse ventricular myocytes, J. Physiol. 518 (1999) 469–478.

[22] L.A. Blatter, J. Huser, E. Rios, Sarcoplasmic reticulum Ca^{2+} release flux underlying Ca^{2+} sparks in cardiac muscle, Proc. Natl. Acad. Sci. U. S. A. 94 (1997) 4176–4181.

[23] G.D. Smith, J.E. Keizer, M.D. Stern, W.J. Lederer, H. Cheng, A simple numerical model of calcium spark formation and detection in cardiac myocytes, Biophys. J. 75 (1998) 15–32.

[24] L.T. Izu, W.G. Wier, C.W. Balke, Theoretical analysis of the Ca^{2+} spark amplitude distribution, Biophys. J. 75 (1998) 1144–1162.

[25] L.T. Izu, J.R. Mauban, C.W. Balke, W.G. Wier, Large currents generate cardiac Ca^{2+} sparks, Biophys. J. 80 (2001) 88–102.

[26] V. Lukyanenko, I. Györke, S. Subramanian, A. Smirnov, T.F. Wiesner, S. Györke, Inhibition of Ca(2+) sparks by ruthenium red in permeabilized rat ventricular myocytes, Biophys. J. 79 (2000) 1273–1284.

[27] C. Soeller, M.B. Cannell, Estimation of the sarcoplasmic reticulum Ca^{2+} release flux underlying Ca^{2+} sparks, Biophys. J. 82 (2002) 2396–2414.

[28] D. Terentyev, S. Viatchenko-Karpinski, H.H. Valdivia, A.L. Escobar, S. Györke, Luminal Ca^{2+} controls termination and refractory behavior of Ca^{2+}-induced Ca^{2+} release in cardiac myocytes, Circ. Res. 91 (2002) 414–420.

[29] S.Q. Wang, M.D. Stern, E. Rios, H. Cheng, The quantal nature of Ca^{2+} sparks and in situ operation of the ryanodine receptor array in cardiac cells, Proc. Natl. Acad. Sci. U. S. A. 101 (2004) 3979–3984.

[30] G.A. Langer, A. Peskoff, Calcium concentration and movement in the diadic cleft space of the cardiac ventricular cell, Biophys. J. 70 (1996) 1169–1182.

[31] C. Soeller, M.B. Cannell, Numerical simulation of local calcium movements during L-type calcium channel gating in the cardiac diad, Biophys. J. 73 (1997) 97–111.

[32] M. Jafri, J.J. Rice, R.L. Winslow, Cardiac Ca^{2+} dynamics: the roles of ryanodine receptor adaptation and sarcoplasmic reticulum load, Biophys. J. 74 (1998) 1149–1168.

[33] R. Hinch, J.L. Greenstein, A. Tanskanen, L. Xu, R.L. Winslow, A simplified local control model of calcium induced calcium release in cardiac ventricular myocytes, Biophys. J. 87 (2004) 3723–3736.

[34] J.J. Rice, M.S. Jafri, R.L. Winslow, Modeling gain and gradedness of Ca^{2+} release in the functional unit of the cardiac diadic space, Biophys. J. 77 (1999) 1871–1884.

[35] J.L. Greenstein, R.L. Winslow, An integrative model of the cardiac ventricular myocyte incorporating local control of Ca^{2+} release, Biophys. J. 83 (2002) 2918–2945.

[36] E.A. Sobie, K.W. Dilly, J. dos Santos Cruz, W.J. Lederer, M.S. Jafri, Termination of cardiac Ca^{2+} sparks: an investigative mathematical model of calcium-induced calcium release, Biophys. J. 83 (2002) 59–78.

[37] M.B. Cannell, C. Soeller, Numerical analysis of ryanodine receptor activation by L-type channel activity in the cardiac muscle diad, Biophys. J. 73 (1997) 112–122.

[38] R. Mejia-Alvarez, C. Kettlun, E. Rios, M. Stern, M. Fill, Unitary Ca^{2+} current through cardiac ryanodine receptor channels under quasi-physiological ionic conditions, J. Gen. Physiol. 113 (1999) 177–186.

[39] C. Kettlun, A. Gonzalez, E. Rios, M. Fill, Unitary Ca^{2+} current through mammalian cardiac and amphibian skeletal muscle ryanodine receptor channels under near-physiological ionic conditions, J. Gen. Physiol. 122 (2003) 407–417.

[40] H. Tanaka, K. Nishimaru, T. Sekine, T. Kawanishi, R. Nakamura, K. Yamagaki, K. Shigenobu, Two-dimensional millisecond analysis of intracellular Ca2+ sparks in cardiac myocytes by rapid scanning confocal microscopy: increase in amplitude by isoproterenol, Biochem, Biophys. Res. Commun. 233 (1997) 413–418.

[41] C. Soeller, M.B. Cannell, A numerical study of ryanodine receptor gating in the cardiac diad and comparison with experimental data, Biophys. J. 84 (2003) 432.

[42] I. Zahradník, J. Pavelková, A. Zahradníková, Inactivation of calcium current by permeating calcium ions in simulated channel clusters, Biophys. J. 78 (2000) 103.
[43] S.O. Marx, J. Gaburjakova, M. Gaburjakova, C. Henrikson, K. Ondrias, A.R. Marks, Coupled gating between cardiac calcium release channels (ryanodine receptors), Circ. Res. 88 (2001) 1151–1158.
[44] G.D. Smith, J. Wagner, J. Keizer, Validity of the rapid buffering approximation near a point source of calcium ions, Biophys. J. 70 (1996) 2527–2539.
[45] A. Michailova, A. McCulloch, Model study of ATP and ADP buffering, transport of Ca(2+) and Mg(2+), regulation of ion pumps in ventricular myocyte, Biophys. J. 81 (2001) 614–629.
[46] M.J. Kushmerick, R.J. Podolsky, Ionic mobility in muscle cells, Science 166 (1969) 1297–1298.
[47] J.C. Bernengo, C. Collet, V. Jacquemond, Intracellular Mg^{2+} diffusion within isolated rat skeletal muscle fibers, Biophys. Chem. 89 (2001) 35–51.
[48] V.L. Pecoraro, J.D. Hermes, W.W. Cleland, Stability constants of Mg^{2+} and Cd^{2+} complexes of adenine nucleotides and thionucleotides and rate constants for formation and dissociation of MgATP and MgADP, Biochemistry 23 (1984) 5262–5271.
[49] S.M. Baylor, S. Hollingworth, Model of sarcomeric Ca^{2+} movements, including ATP Ca^{2+} binding and diffusion, during activation of frog skeletal muscle, J. Gen. Physiol. 112 (1998) 297–316.
[50] D.M. Bers, Excitation–Contraction Coupling and Cardiac Contractile Force, Kluwer, Boston, 2001.
[51] L. Garfinkel, R.A. Altschuld, D. Garfinkel, Magnesium in cardiac energy metabolism, J. Mol. Cell. Cardiol. 18 (1986) 1003–1013.
[52] R.D. Handy, I.F. Gow, D. Ellis, P.W. Flatman, Na-dependent regulation of intracellular free magnesium concentration in isolated rat ventricular myocytes, J. Mol. Cell. Cardiol. 28 (1996) 1641–1651.
[53] J.W. Bassani, R.A. Bassani, D.M. Bers, Relaxation in rabbit and rat cardiac cells: species-dependent differences in cellular mechanisms, J. Physiol. 476 (1994) 279–293.
[54] I. Valent, A. Zahradníková, I. Zahradník, An implementation of the VLUGR3 solver for 3D-simulation of the reaction-diffusion processes in the cardiac dyad, in: V. Capasso (Ed.), Mathematical Modelling and Computing in Biology and Medicine, Esculapio, Bologna, 2003, pp. 213–218.
[55] R.J. Winslow, J. Rice, S. Jafri, E. Marbán, B. O'Rourke, Mechanisms of altered excitation–contraction coupling in canine tachycardia-induced heart failure II: model studies, Circ. Res. 84 (1999) 571–586.
[56] J.G. Blom, J.G. Verwer, VLUGR3: A vectorizable adaptive grid solver for PDEs in 3D. I. Algorithmic aspects and applications, Appl. Numer. Math. 16 (1994) 129–156.
[57] J.G. Blom, J.G. Verwer, Algorithm 759: VLUGR3: a vectorizable adaptive grid solver for PDEs in 3D. II. Code description, ACM Trans. Math. Softw. 22 (1996) 329–347.
[58] A.C. Hindmarsh, ODEPACK, a systematized collection of ODE solvers, in: R.S. Stepleman (Ed.), Scientific Computing, Elsevier, Amsterdam, 1983, pp. 55–64.
[59] A. Zahradníková, I. Zahradník, Description of modal gating of the cardiac calcium release channel in planar lipid membranes, Biophys. J. 69 (1995) 1780–1788.
[60] T.R. Shannon, T. Guo, D.M. Bers, Ca^{2+} scraps: local depletions of free $[Ca^{2+}]$ in cardiac sarcoplasmic reticulum during contractions leave substantial Ca^{2+} reserve, Circ. Res. 93 (2003) 40–45.
[61] Z. Kubalova, D. Terentyev, S. Viatchenko-Karpinski, Y. Nishijima, I. Gyorke, R. Terentyeva, D.N. da Cunha, A. Sridhar, D.S. Feldman, R.L. Hamlin, C.A. Carnes, S. Gyorke, Abnormal intrastore calcium signaling in chronic heart failure, Proc. Natl. Acad. Sci. U. S. A. 102 (2005) 14104–14109.
[62] D.X.P. Brochet, D. Yang, A. Di Maio, W.J. Lederer, C. Franzini-Armstrong, H. Cheng, Ca^{2+} blinks: rapid nanoscopic store calcium signaling, Proc. Natl. Acad. Sci. U. S. A. 102 (2005) 3099–3104.